ACS Catalysis

pubs.acs.org/acscatalysis Research Article

Oxophilicity Drives Oxygen Transfer at a Palladium−Silver Interface for Increased CO Oxidation Activity

Vikram Mehar,[⊥] Abdulrahman Almithn,[⊥] Tobias Egle, Ming-Hung Yu, Christopher R. O'Connor, Mustafa Karatok, Robert J. Madix, David Hibbitts, and Jason F. Weaver*

Cite This: https://dx.doi.org/10.1021/acscatal.0c03885 Read Online

ACCESS | Metrics & More | Article Recommendations | Supporting Information

ABSTRACT: A single-layer AgO_x phase grown on Ag(111) efficiently transfers oxygen to Pd domains at room temperature, rendering the Pd-decorated surface highly reactive toward CO oxidation. Oxygen transfer from AgO_x to Pd and the surface reactivity toward CO were investigated as a function of the Pd coverage using X-ray photoelectron spectroscopy, surface infrared spectroscopy of adsorbed CO, temperature-programmed reaction spectroscopy, and density functional theory (DFT) calculations. Our results show that all of the oxygen from the AgO_x layer (~0.375 monolayer) migrates to the surface of Pd during formation of a nearly complete Pd bilayer at 300 K and that the oxygen coverages generated on Pd increase as the Pd cluster size decreases, reaching values that exceed the oxygen concentration in the AgO_x layer by as much as a factor of 2. Experimental measurements and DFT calculations show that preferential binding of oxygen on the edges of the Pd clusters enhances the oxygen coverage on Pd clusters of decreasing size and produces a heterogeneous spatial distribution of oxygen. CO adsorbs in high coverages at 100 K by binding on both the terraces and O-rich edges of the Pd clusters. During subsequent heating, oxidation of the adsorbed CO consumes nearly all of the oxygen that transferred from AgO_x to the Pd domains; in contrast, the pure AgO_x layer exhibits limited reactivity toward CO adsorbed at 100 K. These results demonstrate that differences in oxophilicity drive facile oxygen transfer from Ag to the edges of Pd nanoclusters and thereby give rise to an efficient pathway for CO oxidation on bimetallic PdAg surfaces. The cooperation between the Pd and Ag domains results in near-interfacial chemistry that may be broadly important in catalysis by bimetallic alloys.

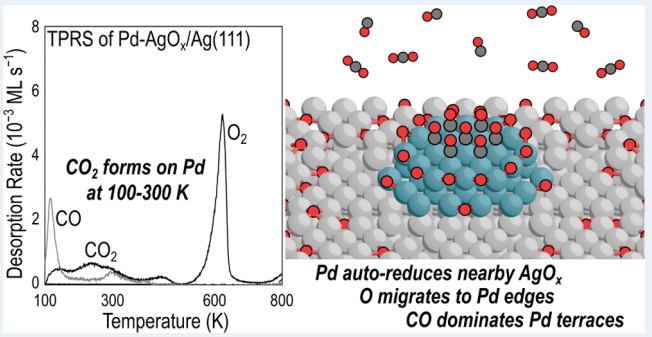

KEYWORDS: *PdAg alloy, alloy catalyst, metal/oxide interfaces, CO oxidation, bifunctional catalysis, PdAg oxidation, CO RAIRS, edge sites*

INTRODUCTION

When used as catalysts for oxidation chemistry, alloys of Pd with Ag (or other coinage metals) can form oxides with relatively low thermodynamic stability, indicating that transitions between the metal and oxide phases can readily occur, even at relatively mild catalysis conditions. In these transitions, transport of oxygen or other species between the various coexisting surface phases can significantly influence the kinetics of heterogeneous catalytic reactions, especially because both Pd and Ag oxides can actively promote catalytic chemistry. Palladium oxide (PdO) is highly active in promoting the dehydrogenation and oxidation of alkanes and other organic species,[1] while O-covered Ag readily promotes complete oxidation reactions as well as partial oxidative transformations of organic species to value-added oxygenates,[2−5] owing to the mobility of O on Ag and electron transfer between O and Ag, leading to a nucleophilic O.[6] The possibility of achieving low-temperature alkane activation on PdO, followed by partial alkyl oxidation on a coexisting Ag phase, provides motivation for exploring PdAg catalysts for potential applications in selective alkane oxidation. In such applications, the exchange of oxygen between the coexisting Pd and Ag phases and the spatial arrangement of adsorbates on these domains may play a central role in determining the catalytic performance and is thus important to understand.

Oxygen atoms are highly mobile during oxidation chemistry on PdO(101) and AgO_x surfaces at mild temperatures. For example, subsurface O-atoms efficiently heal surface O-vacancies created on PdO(101) during CO oxidation and also readily migrate to metallic Pd domains that are generated after more extensive PdO reduction by CO at temperatures

Received: September 6, 2020
Revised: October 26, 2020

https://dx.doi.org/10.1021/acscatal.0c03885
ACS Catal. XXXX, XXX, XXX−XXX

between ~400 and 500 K.[7−10] Also, CO oxidation on an oxidized Ag(111) surface occurs by a similar autocatalytic mechanism wherein the AgO_x phase supplies oxygen to metallic areas that promote CO oxidation at 300 K.[5] These prior studies establish that O-atoms in Pd and Ag oxides migrate rapidly in response to gradients in oxygen chemical potential at moderate temperatures and act to sustain the catalytic oxidation processes that created such gradients.

Oxygen exchange between coexisting Pd and Ag phases may also play an important role in mediating oxidation chemistry on PdAg bimetallic catalysts under oxidizing conditions. Indeed, prior investigations demonstrate that the reduction of oxidized Pd/Ag(111) by H_2 is mediated by H and possibly O transfer between the coexisting Pd and Ag phases.[11,12] A recent study also shows that a single-layer AgO_x structure on Ag(111) efficiently transfers oxygen to Pd during deposition at 300 K,[13] suggesting the possibility that oxygen migration from Ag to Pd provides a pathway for oxygen to participate in catalytic oxidation reactions on PdAg bimetallic surfaces. Overall, the fundamental understanding of oxygen-exchange processes in PdAg bimetallics and their influence on surface reactivity is generally lacking, due in large part to challenges in preparing well-defined oxide structures on PdAg surfaces for controlled investigations.

In the present study, we investigated oxygen transfer from AgO_x to Pd and the CO oxidation activity of surfaces prepared by depositing Pd on a well-ordered single-layer AgO_x/Ag(111) surface. A key aim of this work is to investigate how the Pd cluster size influences the oxygen-transfer process and the subsequent surface reactivity. Our results demonstrate that differences in oxophilicity promote facile O transfer from AgO_x to Pd and efficient oxidation of adsorbed CO. Significantly more efficient oxygen transfer and higher CO oxidation activity (per Pd) are identified for Pd bilayer clusters of decreasing size and are shown to originate from optimal accessibility to oxygen from the surrounding AgO_x as well as enhanced stabilization of oxygen at edge sites of the Pd clusters.

EXPERIMENTAL DETAILS

Temperature-programmed reaction spectroscopy (TPRS) and reflection−absorption infrared spectroscopy (RAIRS) measurements were performed in an ultrahigh vacuum (UHV) system that has been described previously.[8] The UHV chamber is equipped with a scanning tunneling microscope (RHK), a four-grid retarding field analyzer (SPECS) for low-energy electron diffraction (LEED) and Auger electron spectroscopy (AES), a quadrupole mass spectrometer (QMS) (Hiden) used for TPD and TPRS experiments, a Fourier transform infrared spectroscopy system for RAIRS measurements, an ion sputter gun, and an electron beam metal evaporator (McAllister Technical Services) for vapor deposition of Pd. A single-stage differentially pumped chamber[14] is also attached to the main UHV chamber, which houses an inductively coupled RF plasma source that is used to generate atomic oxygen beams. Details of the sample support structure and cleaning methods are given in the Supporting Information and have been reported previously.[13]

A single-layer AgO_x film containing 0.38 ML (monolayer) of oxygen was grown by exposing the Ag(111) surface to an O-atom beam at a surface temperature of 515 K, followed by heating to 535 K in UHV. The O_2 TPD spectrum obtained from the single-layer AgO_x/Ag(111) surface exhibits a sharp peak at 570 K (Figure S1). As shown previously,[13] the oxidation procedure employed produces a well-ordered AgO_x single layer composed of three crystalline structures with distinct long-range arrangements but similar local structural motifs; the models of these crystal structures are shown in Figure S2. Each structure has an oxygen density between 0.375 and 0.40 ML, where 1 ML is equal to the surface atom density of Ag(111). Films of varying Pd thickness were grown on the AgO_x/Ag(111) surface at 300 K by vapor depositing Pd (Alfa Aesar, 99.9%) using an electron beam evaporator. The Pd coverage was calibrated by collecting the AES spectra as a function of Pd exposure to clean Ag(111) at 300 K and relating the attenuation of the Ag MNN peak at 351 eV to the thickness of the Pd layer, assuming an inelastic mean free path (IMFP) of the Auger electrons through Pd of 7.05 Å as estimated by the Gries equation.[15] Coverages of Pd are reported in units of ML by dividing the thickness estimated from the AES measurements with the monatomic step height on Pd(111) of 2.2 Å. The average Pd deposition rate was 0.075 ML/min for our measurements.

After depositing Pd on the single-layer AgO_x film, the sample was cooled to 100 K and saturated with CO using background dosing for 15 min at a CO partial pressure of 5×10^{-9} Torr, which corresponds to a CO exposure of 4.5 Langmuir (L). TPRS and CO RAIRS measurements show that CO saturation coverages are obtained on the clean and Pd-covered AgO_x surfaces at 100 K for CO exposures above about 3 L. TPRS measurements were performed with the sample positioned ~5 mm from the entrance aperture to the QMS, and the partial pressures of CO, O_2, and CO_2 (m/z = 28, 32, and 44) were monitored while heating at a constant rate of 1 K/s until the sample temperature reached 800 K. Fragmentation of CO_2 in the QMS produces a 28 amu signal that is only about 10% of the 44 amu signal and is taken into account in our quantitative analysis. The O_2 TPD yields obtained from Pd−AgO_x/Ag(111) surfaces were calibrated by assuming that growth of the pure, single-layer AgO_x/Ag(111) structure at 500 K saturates at an oxygen coverage of 0.38 ML.[16−18] An optimal scaling factor for converting integrated CO_2 TPRS spectra to units of ML of CO_2 was determined by assuming that all of the initial 0.38 ML of oxygen desorbs from the surface as either O_2 or CO_2 during TPRS at Pd coverages below 2 ML. Last, CO TPRS yields were computed using the CO_2 scaling factor divided by 1.3, where the proportionality between the CO and CO_2 TPRS scaling factors was determined in recent experiments performed in our apparatus.[19]

Scanning tunneling microscopy (STM) measurements were performed at a sample temperature of ~300 K, and the tunneling interaction was set to the constant current feedback mode. Images were collected at typical scan settings in the range of +0.2 to +0.5 V sample bias and a tunneling current of 0.5−1.2 nA. RAIRS measurements were performed at a sample temperature of 100 K, and a nonpolarized IR beam was reflected from the sample at an incident angle of ~80° from the surface normal. All of the reported RAIRS spectra are an average of 512 scans and were collected at a 4 cm^{-1} resolution.

COMPUTATIONAL METHODS

Periodic plane wave density functional theory (DFT) calculations were performed using the Vienna *Ab Initio* simulation package (VASP)[20−23] as implemented in the Computational Catalysis Interface (CCI).[24] Plane waves were constructed using projector augmented wave potentials

https://dx.doi.org/10.1021/acscatal.0c03885
ACS Catal. XXXX, XXX, XXX−XXX

with an energy cutoff of 396 eV.[25,26] The revised Perdew−Burke−Ernzerhof form of the generalized gradient approximation was used to describe the exchange and correlation energies.[27−29] Wave functions were converged until the electronic energies varied less than 10^{-6} eV. Forces on all atoms were determined using a fast Fourier transform grid with a cutoff equal to twice the plane wave cutoff and structures were geometrically optimized until the forces on all atoms were less than 0.05 eV $Å^{-1}$.

Prior work[13,16−18,30,31] has shown that single-layer AgO_x films on the Ag(111) surface can have three different structures with a stoichiometry close to Ag_2O: hexagonal $p(4 \times 4)$ structure (Figure 1a), rectangular $c(3 \times 5\sqrt{3})$ structure, and

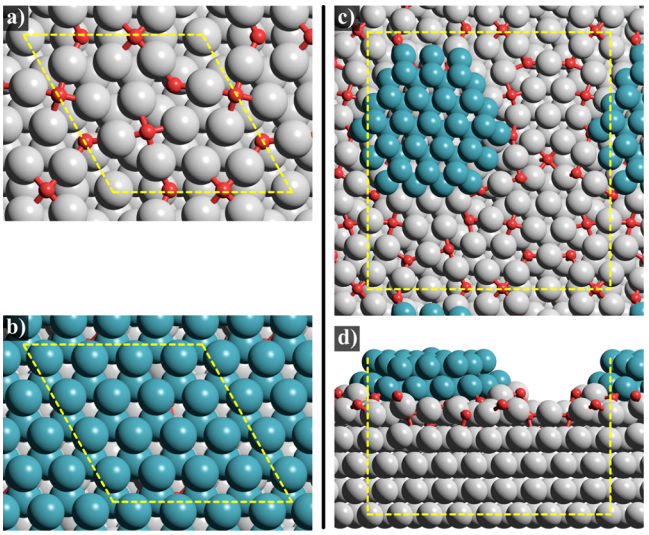

Figure 1. (a) Top view of Ag_2O−$p(4 \times 4)$-Ag(111) without Pd, (b) 4 × 4 bilayer Pd overlayer on Ag_2O−$p(4 \times 4)$-Ag(111), and (c,d) top and side views of the bilayer Pd_{46} hemispherical particle on Ag_2O−$p(4 \times 5\sqrt{3})$-Ag(111). Color code: O (red), Ag (gray), and Pd (dark cyan). A supercell of 2 × 1 was used for the Ag_2O−$p(4 \times 5\sqrt{3})$ phase to accommodate the Pd_{46} particle. Yellow dashed lines show the unit cell for each model. All atoms except the adsorbed CO were constrained during frequency calculations.

rectangular $p(4 \times 5\sqrt{3})$ structure as shown in Figure S2. These models were constructed with four-layer thick Ag(111) slabs. The conformal Pd bilayer (Figure 1b) was modeled by a 4 × 4 Ag(111) surface with four layers orthogonal to the surface, the $p(4 \times 4)$ Ag_2O structure, and then two layers of Pd above that with 20 Å of vacuum separating slabs. The lattice parameter for the 4 × 4 Ag(111) surface is 11.553 Å compared to 11.005 Å for 4 × 4 Pd(111), resulting in a lattice mismatch of ∼5%. Previous studies have shown that the lattice strain can modify the electronic properties of metal surfaces.[32] However, here, we also used a Pd cluster model (described next) where Pd clusters and AgO_x surface are completely unconstrained, eliminating any unnatural strains. Similar conclusions were obtained from both models, suggesting that the effects of the lattice mismatch in the conformal Pd bilayer model used here is minimal. For the bilayer Pd clusters, a 2 × 1 super cell of the $p(4 \times 5\sqrt{3})$ structure was used above four layers of rectangular 8 × 10 Ag(111) surface (23 × 25 Å) with 15 Å of vacuum. A bilayer hemispherical Pd_{46} particle (1.38 nm in diameter), which predominantly exposes a Pd(111) surface and is truncated by alternating (111) and (100) facets, was then placed on top of the Ag_2O layer (Figure 1c,d). The bottom two Ag(111) layers were fixed in their bulk positions in both models and all other atoms were relaxed during geometric convergence.

A 3 × 3 × 1 Monkhorst−Pack sampling of the first Brillouin zone (*k*-point mesh)[33,34] was used during the geometric convergence for the conformal Pd bilayer model and a 1 × 1 × 1 *k*-point mesh was used for the bilayer Pd cluster model. After geometric convergence, single-point calculations with 6 × 6 × 1 and 2 × 2 × 1 *k*-point meshes for the conformal and cluster models, respectively, were performed to determine the electronic energy. Frequency calculations were performed to determine the C−O stretch frequency using the harmonic oscillator approximation; all atoms except the adsorbed CO were constrained during these calculations.

RESULTS AND DISCUSSION

Morphology and Auto-Oxidation of Pd Deposited on AgO_x/Ag(111). Knowledge of the growth, morphology, auto-oxidation, and fractional coverage of Pd deposited onto AgO_x/Ag(111) is required for interpreting the CO adsorption and oxidation behavior on the Pd−AgO_x/Ag(111) surfaces, with AgO_x containing 0.38 ML O. For relatively low amounts of deposited Pd, uniformly dispersed Pd clusters (∼2.5−3 nm) form across the AgO_x surface (Figure 2a), whereas a well-

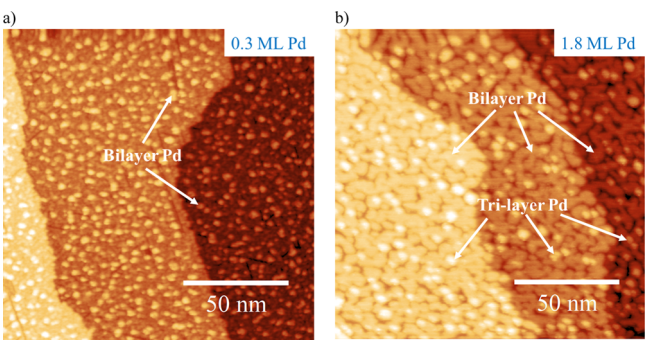

Figure 2. STM images (150 × 150 nm) obtained after depositing Pd on the single-layer AgO_x/Ag(111) surface at 300 K to generate Pd coverages of (a) 0.30 ML (444 mV, 0.83 nA) and (b) 1.8 ML (241 mV, 0.69 nA). In image (a), the small, bright features (arrows) correspond to bilayer Pd clusters that are dispersed on top of the AgO_x layer. A well-connected Pd bilayer is the dominant structure in image (b) and the bright features on each terrace correspond to a minority amount of Pd trilayer domains. Three monatomic step edges of the Ag(111) surface are evident in both images.

connected bilayer Pd film forms at higher Pd loading (Figure 2b).[13] Approximately 10% of the higher coverage structure consists of domains that are three layers high (Figure 2b, bright spots).

STM images demonstrate a transition from single to bilayer Pd cluster growth as the Pd coverage is increased above ∼0.15 ML as well as the dominance of bilayer growth between ∼0.3 and 2 ML.[13] As reported previously, quantitative analysis of STM images shows that the fraction of the surface covered by Pd increases in approximately 1:1 proportion with increasing Pd coverage to 0.15 ML but increases in about 1:2 proportion with increasing Pd coverage from 0.3 to 1.8 ML.[13] To illustrate this relationship, Table 1 lists the total Pd coverage (ML), the fraction of the surface covered by Pd, and the average diameters of the Pd domains (determined previously from STM) for each of the surfaces studied here.[13] Hereafter, the

https://dx.doi.org/10.1021/acscatal.0c03885
ACS Catal. XXXX, XXX, XXX−XXX

Table 1. Total Coverage of Pd (ML) Deposited on the AgO_x/Ag(111) Surface, Surface Coverage of Pd (ML-surfPd), and the Average Diameters of Pd Domains for Surfaces Investigated in This Work[a]

Pd (ML)	0.15	0.30	0.45	0.90	1.35	1.8
Pd (ML-surfPd)	0.19	0.18	0.21	0.49	0.71	0.95
D_{avg} (nm)	1.4	2.7	2.8	6.4		32.8

[a]The surface Pd coverages and average diameters were determined from statistical analysis of STM images as reported previously.[13] The total coverage represents the total amount of Pd projected onto a unit area of the Ag(111) substrate, while the surface coverage represents the coverage of Pd located at the vacuum−solid interface or the Pd−AgO_x interface. Units of ML and ML-surfPd are both scaled to the surface atom density of the Ag(111) surface.

fraction of the surface covered by Pd is referred to as the surface Pd coverage because this fraction is proportional to both the number of Pd atoms at the vacuum−solid interface and the number of Pd atoms in direct contact with the Ag substrate. The surface Pd coverage is expressed in units of ML-surfPd, where 1 ML-surfPd corresponds to a single layer of Pd atoms with the same areal density as Ag(111) covering the entire Ag(111) substrate. For 0.15 ML of Pd, the total and surface Pd coverages are approximately equal because single-layer clusters are dominant, whereas the surface Pd coverage is approximately half of the total Pd coverage at higher coverage (Table 1) because bilayer clusters are dominant in this regime.[13] It is important to note that units of ML-surfPd underestimate the number of Pd atoms at the vacuum−solid interface because this scale is based on the total area of the Ag(111) surface covered by Pd and neglects Pd atoms at the edges of clusters. Relationships between the coverages of Pd edge and terrace sites for bilayer clusters of varying size are given in the Supporting Information (Section S4, Table S1) and discussed further below. Distinguishing the total and surface Pd coverages is important for understanding the auto-oxidation and reactivity of Pd on AgO_x.

Recently published work using X-ray photoelectron spectroscopy (XPS) demonstrates that the AgO_x layer efficiently transfers oxygen to the Pd at 300 K and that the amount of Pd affected by oxygen varies with the Pd coverage.[13] In the present study, the amount of oxygen transferred to Pd was estimated by analyzing differences between O 1s spectra obtained before and after Pd deposition onto the AgO_x layer (Section S5; Table S3). The analysis assumes that diminution of the O 1s peak from the AgO_x phase is caused solely by oxygen transfer from the AgO_x to Pd. In support of this assumption, we estimate that inelastic scattering of photoelectrons by the deposited Pd could account for only about 20% of the observed decrease in the O 1s peak from AgO_x (see Section S5). Additionally, analysis of the Pd 3d spectra shows that the amount of Pd that is oxidized agrees well with the amount of oxygen depletion from the AgO_x phase determined from the O 1s difference spectra (Table S3).

The XPS analysis shows that the total amount of oxygen transferred to Pd increases as the Pd coverage is increased to ∼2 ML, at which point the Pd bilayer nearly completely covers the surface (Table 1) and all of the oxygen from the AgO_x layer has migrated to Pd (Figure 3, black). The analysis further shows that the surface O coverage on Pd single-layer clusters ([Pd] < 0.15 ML) is less than the oxygen coverage in the underlying AgO_x layer (dashed line) but increases by more than a factor of 2 as the Pd coverage is increased to ∼0.25 ML

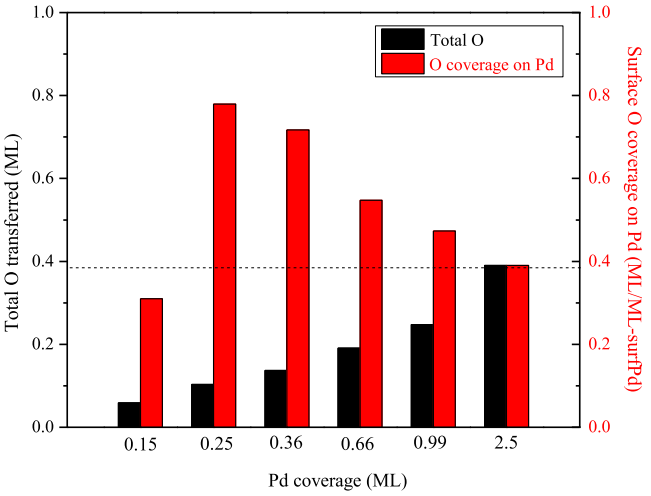

Figure 3. Total amount of oxygen (black) transferred from the AgO_x layer to Pd and the resulting surface coverage of oxygen on Pd (red) as a function of the total Pd coverage (ML) deposited onto AgO_x at 300 K. The dashed line represents the initial oxygen coverage in the AgO_x layer (∼0.38 ML). The total amount of oxygen transferred (ML) was estimated from an analysis (section S5) of XPS Pd 3d and O 1s spectra reported previously.[13] The oxygen coverage on the Pd clusters was then estimated by dividing the total amount of O transferred by the surface coverage of Pd, where the latter was estimated from analysis of STM images reported previously (e.g., Table 1).[13] Single-layer Pd clusters form at total Pd coverages below ∼0.15 ML, and bilayer clusters become dominant at higher Pd coverages, until a conformal bilayer is completed at a total Pd coverage of ∼2 ML. The Pd surface coverage is approximately equal to 100 and 50% of the total Pd coverage for single and bilayer clusters (Table 1), respectively.

and small bilayer Pd clusters become dominant (Figure 3, red). The amount of oxygen transferred to the small Pd bilayer clusters (∼0.75 ML O/ML-surfPd) is also approximately 2 times larger than the amount of oxygen available in the portion of the AgO_x layer that makes direct contact with the Pd, demonstrating that at least half of the oxygen migrated to Pd from uncovered areas of the AgO_x layer.[13] In this case, even though ∼13% of the surface is covered by Pd, oxygen transfer to the Pd completely reduces the equivalent of 25% of the AgO_x. Based on the total amount of oxygen in the AgO_x layer, oxygen transfer to Pd could maintain an O coverage of 0.75 ML/ML-surfPd for total Pd coverages up to 1 ML, for example, $[O]_{max}$ on 1 ML Pd ∼ (0.38 ML O)/(0.5 ML-surfPd). Instead, however, the O coverage on surface Pd begins to decrease as the Pd coverage is increased from ∼0.4 to 1 ML (Figure 3, red), suggesting that the O transfer becomes less effective as the Pd domains grow in size. Overall, these results demonstrate that the O transfer from AgO_x to Pd is highly facile. All of the oxygen from the AgO_x layer migrates to Pd during the formation of a nearly complete bilayer at [Pd] ∼ 2 ML, and oxygen transfer to smaller bilayer domains ([Pd] < 2 ML) produces O coverages on the Pd which exceed that in the underlying AgO_x layer by as much as a factor of 2, indicating that Pd reduces a greater proportion of the AgO_x layer than it covers.

Energetics of Oxygen Transfer from AgO_x to Pd and Preferred Binding Sites. DFT-calculated energies predict a strong thermodynamic driving force for O atoms to move from a $p(4 \times 4)$ AgO_x surface (Figure 1a) to the top of a conformal Pd bilayer surface (Figure 4). Six O atoms exist in the $p(4 \times 4)$

https://dx.doi.org/10.1021/acscatal.0c03885
ACS Catal. XXXX, XXX, XXX−XXX

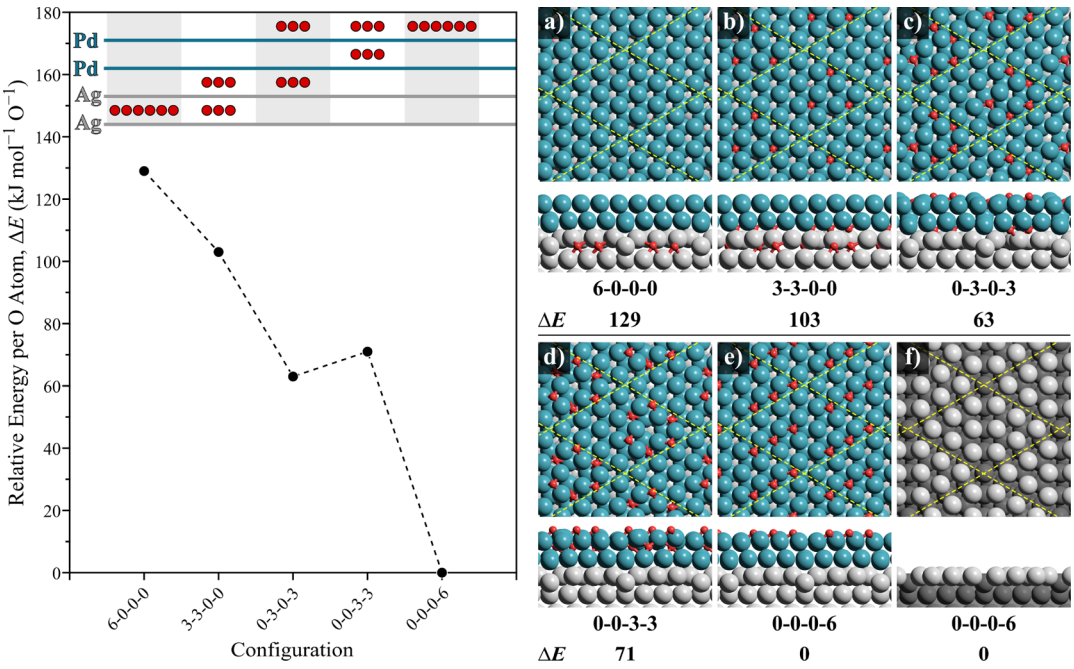

Figure 4. (Left) DFT-predicted relative energies, normalized per O atom, for O configurations on the 4 × 4 bilayer Pd overlayer on the AgO_x surface. (Right) Optimized structures shown for each O configuration (a–e). The image in (f) shows the arrangement of Ag atoms beneath the Pd bilayer after all oxygen atoms moved to the first Pd layer as shown in (e). Color code: O (red), Ag (gray), and Pd (dark Cyan).

AgO_x surface, and five different configurations of these O atoms in the Pd bilayer model (Figure 1b) were examined by moving the O atoms from the AgO_x layer into the Pd region of the conformal Pd bilayer. Relative energies demonstrate that having the six O on top of the Pd bilayer is 129 kJ mol^{-1} O^{-1} more stable than their original location within the surface Ag layer (as Ag_2O, Figure 1a without Pd, Figure 1b with a Pd bilayer). A similar thermodynamic driving force promotes O migration to the surface of the conformal Pd single-layer models, as shown in Figure S5 (Section S6). The energy per oxygen atom decreases in a nearly monotonic fashion as the oxygen atoms beneath the AgO_x layer move to the surface of the Pd bilayer. This relative energy decreases from 129 kJ mol^{-1} in the "6–0–0–0" configuration (where this notation indicates that all six O atoms are in the Ag layer, Figure 4a) to 103 kJ mol^{-1} when half of the oxygen atoms are between the AgO_x layer and the bottom Pd layer (3-3-0–0; Figure 4b) and decreases further to 63 kJ mol^{-1} for the 0–3–0–3 configuration (Figure 4c). The 0–3–3–0 configuration was attempted, but it spontaneously changes to the 0–3–0–3 configuration during structural relaxation, demonstrating the instability of O atoms in the interstitial regions between two close-packed Pd layers. In contrast, the AgO_x layer has a lower density of Ag atoms compared with the Pd, enabling the oxygen atoms to reside between the AgO_x layer and the bottom Pd layer. This is also evident by the slightly higher energy of 0–0–3–3 relative to the 0–3–0–3 configuration (Figure 4c,d) before the significant decrease (71 kJ mol^{-1}O^{-1}) upon moving the remaining three, subsurface oxygen atoms to the surface of the Pd bilayer (Figure 4e).

When all six oxygen are on the surface, in the same positions that they reside in the surface of AgO_x, the relative energy (per oxygen atom) is 61 kJ mol^{-1} O^{-1} lower than that of the "0–0–3–3" structure and 118 kJ mol^{-1} O^{-1} lower than that of the "6–0–0–0" structure (where O resides in the AgO_x layer). This demonstrates that a strong thermodynamic driving force stimulates the migration of O atoms to the Pd surface; however, it neglects the ability of the O atoms to rearrange in such a process. To determine the most stable configuration of six O atoms on the Pd surface, we examined a total of 434 unique configurations (out of a total of 1,626), with this sampling prioritizing structures with large average O–O distances. Figure S6 shows the relative energies of these unique configurations as a function of the average O–O distance; the energy decreased by ∼160 kJ mol^{-1} with increasing the average O–O distance from 3.84 to 5.86 Å. The energy also varies significantly at a given average O–O distance, showing a strong preference for fcc sites compared to hcp sites. For example, at an average O–O distance of ∼5.86 Å, placing all six oxygen atoms on 3-fold fcc sties is 41 kJ mol^{-1} more favorable than distributing the oxygen atoms evenly on both fcc and hcp sites. The most stable configuration of the "0–0–0–6" arrangement with an average O–O distance of 5.86 Å is shown in Figure 4e.

In addition to the five different O configurations shown in Figure 4, we tested two additional configurations, 0–1–0–5 and 0–0–1–5 to examine the effects of O–O repulsion on the Pd surface on O migration as shown in Figure S7 (Section S7; Supporting Information). The 0–1–0–5 configuration is 14 kJ mol^{-1} O^{-1} less favorable than the 0–0–0–6 configuration, while the difference between 0–0–1–5 and 0–0–0–6 is insignificant (∼3 kJ mol^{-1} O^{-1} in favor to 0–0–1–5). This suggests that O may reside in subsurface positions to alleviate O–O repulsive interactions at high O coverages on the Pd surface. However, the slight preference of a single O atom to reside within the Pd bilayer could be artificially induced by the 5% stretch of the Pd(111) lattice present in this model as discussed in the Computational Methods section. Overall, DFT demonstrates that oxygen migration from the AgO_x surface to a conformal Pd bilayer is thermodynamically favored by 129 kJ mol^{-1} O^{-1} (774 kJ mol^{-1} total) and that the oxygen

https://dx.doi.org/10.1021/acscatal.0c03885
ACS Catal. XXXX, XXX, XXX–XXX

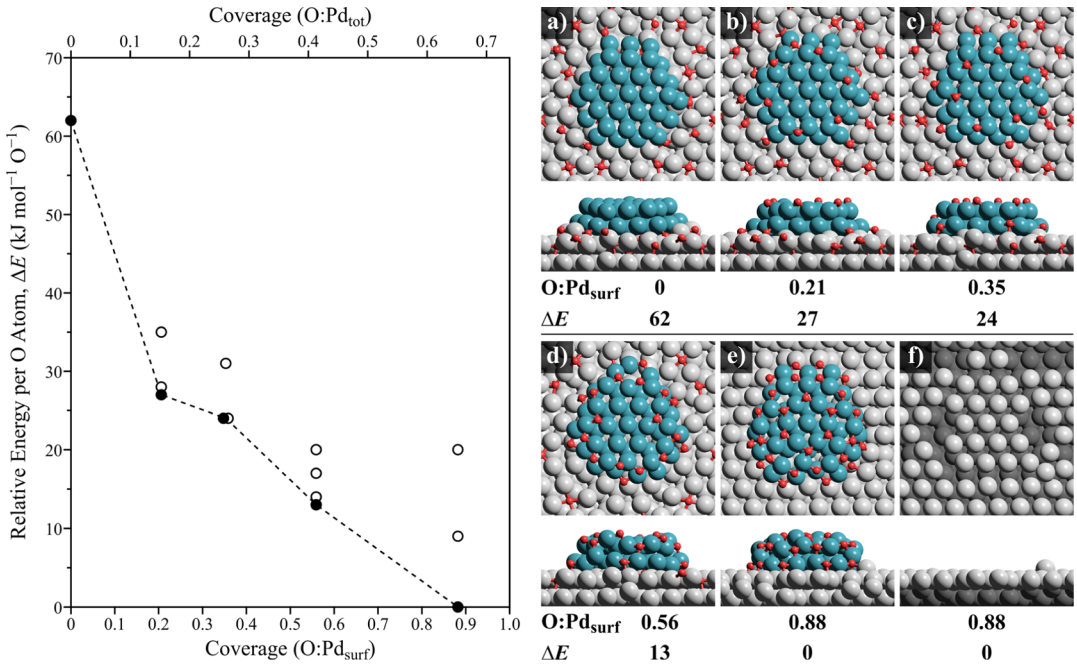

Figure 5. (Left) DFT-predicted relative energies, normalized per O-atom, for O configurations on the bilayer Pd_{46} hemispherical particle on the AgO_x surface as a function of O coverage on the surface of the Pd particle, shown per surface Pd (bottom axis) and total Pd atom (top axis). Multiple O configurations were examined at each coverage, and the most stable configurations at each coverage are shown in closed symbols while all other configurations are shown in open symbols. (Right) Optimized structures shown for the most stable O configurations at each O coverage on Pd (a–e). The image in (f) shows the arrangement of Ag atoms beneath the Pd_{46} particle after all oxygen atoms moved to Pd as shown in (e). Color code: O (red), Ag (gray), and Pd (dark cyan). Structures for the other configurations are shown in Figure S8 in the Supporting Information.

strongly prefers to reside on the surface of the Pd within spatially distributed fcc sites.

These large thermodynamic driving forces suggest that oxidation of the Pd domains and concurrent reduction of the AgO_x located directly below the Pd is exothermic. XPS results, however, demonstrate that the oxygen coverages on Pd pass through a maximum as the Pd coverage increases (Figure 3), suggesting that Pd clusters reduce the AgO_x surface directly beneath them and some of the surrounding AgO_x. For example, Pd clusters covering about 25% of the AgO_x surface will reduce 50% of the AgO_x. Furthermore, conformal bilayers are only present at a total Pd coverage of ~2 ML (Figure 2); at lower Pd coverages, bilayer Pd clusters exist, which expose a significant amount of undercoordinated Pd edge and corner atoms that may stabilize O beyond the Pd(111) surfaces modeled in the conformal structure.

DFT predicts that oxygen atoms transferred from AgO_x preferentially bind on the edges of bilayer Pd clusters and indeed suggests that a fractional coverage of Pd bilayer clusters can thermodynamically induce complete reduction of the AgO_x layer. Oxygen transfer to bilayer Pd clusters was examined using a model of a Pd_{46} bilayer cluster on a 2 × 1 super cell of the $p(4 \times 5\sqrt{3})$ AgO_x surface ($Ag_{64}O_{30}$ surface) (Figure 1c,d); this Pd_{46} cluster covers 35% of the underlying AgO_x surface. Multiple configurations of oxygen on the Pd_{46} cluster were examined for several extents of O migration, that is, at different O/Pd_{surf} coverages, where Pd_{surf} is equal to the number of Pd atoms at the top surface and edges. Notably, oxygen coverages given in units of ML/ML-surfPd (such as Figure 3) are greater than the O/Pd_{surf} ratios shown here because the latter account for Pd atoms at both terrace and edge sites (Section S4; Table S2). The DFT-calculated energies decrease by 35 kJ mol^{-1} O^{-1} (normalized per total oxygen atom) as the seven oxygen atoms beneath the Pd cluster (Figure 5a) diffuse to the Pd surface (Figure 5b), representing a coverage of 0.21 O/Pd_{surf} (Figure 5). For an oxygen coverage of 0.21 O/Pd_{surf}, DFT predicts that the bridging sites along the edges in the top layer of the Pd cluster (Figure 5b) are slightly more favorable for binding oxygen than the terrace hollow sites and much more favorable than the bridging sites on the edges of the bottom Pd layer (Figure S8; Supporting Information).

Moving oxygen atoms from uncovered areas of the AgO_x layer to Pd continues to be thermodynamically favored up to an oxygen coverage of at least 0.88 O/Pd_{surf} (Figure 5, left), at which point, all 30 O atoms have migrated from the AgO_x layer to the surface of the Pd (Figure 5e). Notably, the Ag atoms in the underlying AgO_x layer spontaneously rearranged during structural optimization into a structure resembling close-packed Ag(111) and lose their original triangular-shaped Ag_6 and Ag_{10} arrangements upon the migration of all oxygen atoms to Pd (Figure 5f compared to Figure S2, Supporting Information); this same rearrangement of Ag does not happen in the conformal bilayer model (Figure 4f). Bridging sites at the edges of the cluster remain more favorable for binding oxygen than terrace sites between 0.35 and 0.88 O/Pd_{surf} coverages (Figure 5b–d) until these sites become saturated and the remaining oxygen atoms move to terrace sites. Preferential binding on edge sites has also been reported for H and CO on similar Ir, Pt, and Ru nanoparticles[35,36] and is expected to occur in many adsorbate/metal combinations because the greater degree of coordinative undersaturation at edge sites tends to strengthen the adsorbate–metal bonding.

The experimental data shows that O coverages on Pd fail to reach 0.9 O/Pd_{surf} and instead increase to a maximum of ~0.5 O/Pd_{surf} (S4, Table S2), suggesting that kinetic and/or spatial

https://dx.doi.org/10.1021/acscatal.0c03885
ACS Catal. XXXX, XXX, XXX–XXX

limitations prevent the complete migration of all O in the AgO_x domain to the Pd clusters at 300 K. The structure shown in Figure 5d has O preferentially decorating the edges of Pd and a coverage of 0.56 O/Pd_{surf}, close to the measured maximum; this O-covered structure may thus be representative of the small bilayer clusters investigated experimentally. These results, taken alongside the experimental data, suggest that O atoms in AgO_x directly beneath or nearby Pd clusters will migrate to corner and edge atoms of these small Pd clusters, resulting in reduction of the Ag surface and partial surface oxidation of the Pd clusters.

Preferential binding of oxygen on Pd edge sites is expected to cause the O coverage on Pd to increase with decreasing Pd coverage on AgO_x in a manner that closely resembles the behavior observed experimentally (Figure 3). The origin for such behavior is that the actual number of surface Pd sites that project onto a unit area of the Ag(111) substrate increases markedly as the Pd cluster size is decreased because of the contribution of edge sites (S4; Table S1), and as Pd clusters grow, the fraction of Pd at edges decrease and becomes zero for conformal bilayers. The fraction of Pd edge sites can be approximated for clusters of varying size investigated experimentally, thus enabling a more direct comparison between the oxygen coverages on Pd determined from experiment and DFT. From STM data,[13] the average diameters of the bilayer clusters are ~3 and 6 nm at total Pd coverages of 0.30 and 0.90 ML, respectively (Table 1). Assuming that these clusters have the same shape as that modeled using DFT, we estimate that 50 and 30% of the surface Pd atoms are located on the edges of the ~3 versus 6 nm clusters (S4; Table S1); the fraction of Pd edge atoms is about 1.7 times higher for the small versus large clusters in this case. Experimental estimates show that the oxygen coverage on Pd is also higher on the smaller of these clusters by a factor of ~1.7, which is approximately equal to the ratio of the Pd edge site fractions for these clusters. Thus, the oxygen coverage on Pd increases in proportion to the fraction of Pd edge sites for the cluster sizes considered here. Further, after accounting for Pd edge sites for the model cluster geometry (S4; Table S2), the oxygen coverages are estimated to be ~0.49 and 0.33 O/Pd_{surf} on the 3 and 6 nm clusters, respectively, very close in value to the Pd edge site fractions. These quantitative comparisons support the idea that enhanced stabilization of oxygen at edge sites is partly responsible for the enhanced uptake of oxygen by Pd clusters of decreasing size on AgO_x.

Examination of Pd Sites Using CO Adsorption and Infrared Spectroscopy. Reflection absorption IR spectroscopy further demonstrates that the adsorbed oxygen is present on the surfaces of the Pd clusters on AgO_x and provides strong evidence of preferential oxygen binding to the edge sites of the clusters. IR spectra were acquired after adsorbing CO to saturation on Pd-covered AgO_x surfaces at 100 K. As shown below, high CO saturation coverages were generated on the Pd; the CO coverages decrease from ~0.75 to 0.5 CO/Pd_{surf} as the Pd coverage is increased from 0.3 to 1.8 ML. The IR spectra obtained from CO-saturated surfaces exhibit two main C−O stretch bands; the band at 2057−2088 cm^{-1} originates from CO adsorbed in an atop configuration on a Pd atom (CO−Pd species)[37,38] and the band at 2104−2128 cm^{-1} originates from an atop CO−Pd−O species in which the CO is bound to a Pd atom that is also bound to adsorbed O (Figure 6).[10,39,40] DFT calculations performed here predict that the C−O stretch frequency for CO−Pd−O species is

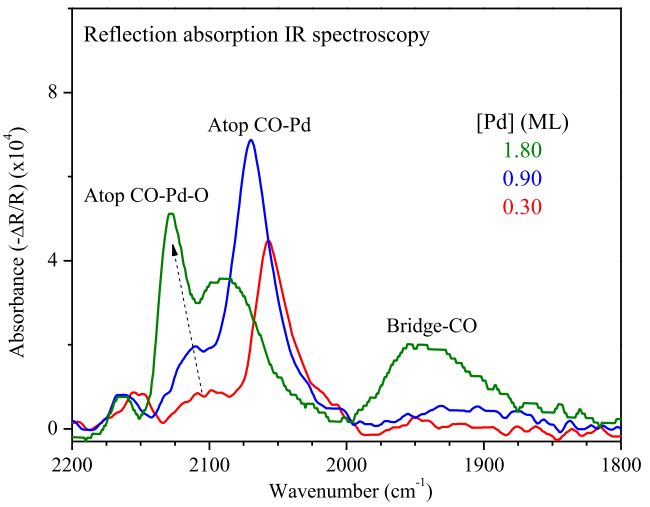

Figure 6. Reflection absorption IR spectra obtained after adsorbing CO to saturation at 100 K on a Pd−AgO_x/Ag(111) surface with 0.3, 0.9, and 1.8 ML of Pd. Figure S10 in the Supporting Information shows IR spectra obtained from other Pd coverages.

similarly blue-shifted relative to the CO−Pd species (Figure S9; Supporting Information). The band at 2160 cm^{-1} is attributed to weakly bound CO on Ag sites,[41−43] and the low intensity below 2000 cm^{-1} for Pd coverages less than ~1 ML demonstrates that CO adsorbs negligibly on the bridge and hollow sites of the small Pd clusters; the emergence of the broad band centered at 1945 cm^{-1} indicates that a fraction of the adsorbed CO binds on the bridge sites of the nearly completed Pd bilayer. The appearance of a C−O stretch band for the CO−Pd−O species indeed confirms that adsorbed oxygen is present on Pd prior to CO adsorption, while the appearance of the band for CO−Pd species demonstrates that a fraction of the adsorbed CO is unaffected by the coadsorbed oxygen. The simultaneous appearance of both C−O stretch bands thus suggests that the Pd clusters are initially covered by separate oxygen-rich and oxygen-depleted regions, consistent with heterogeneity in the oxygen adlayer resulting from preferential accumulation of oxygen on Pd edge sites.

The variation in the relative intensities of the CO−Pd and CO−Pd−O bands with increasing Pd coverage further supports the interpretation that oxygen binds preferentially on the edges of small Pd clusters, leaving the terraces depleted of oxygen. As seen in Figure 6, the relative intensity of the CO−Pd−O band (compared with the CO−Pd band) is quite small for Pd coverages below ~1 ML but increases sharply at higher Pd coverages. This trend is intriguing considering that the oxygen coverage on Pd is highest for the small bilayer Pd clusters and decreases with increasing Pd coverage (Figure 3). Preferential binding of oxygen on the Pd edge sites and a shift of oxygen to the terrace sites as the Pd domain size is increased can account for the variation in the CO−Pd−O band intensity. Assuming that oxygen binds selectively on the edges of the smallest Pd clusters, nearly all of the CO−Pd−O species would be located on edge sites while the CO−Pd species would mainly be present on the terraces. In this case, any CO adsorbates associated with oxygen (CO−Pd−O) would tend to tilt significantly away from the surface normal, and IR absorption by these CO molecules would be weak compared with the more upright standing CO adsorbed on the O-depleted terraces due to the surface selection rule.[44] As a result,

https://dx.doi.org/10.1021/acscatal.0c03885
ACS Catal. XXXX, XXX, XXX−XXX

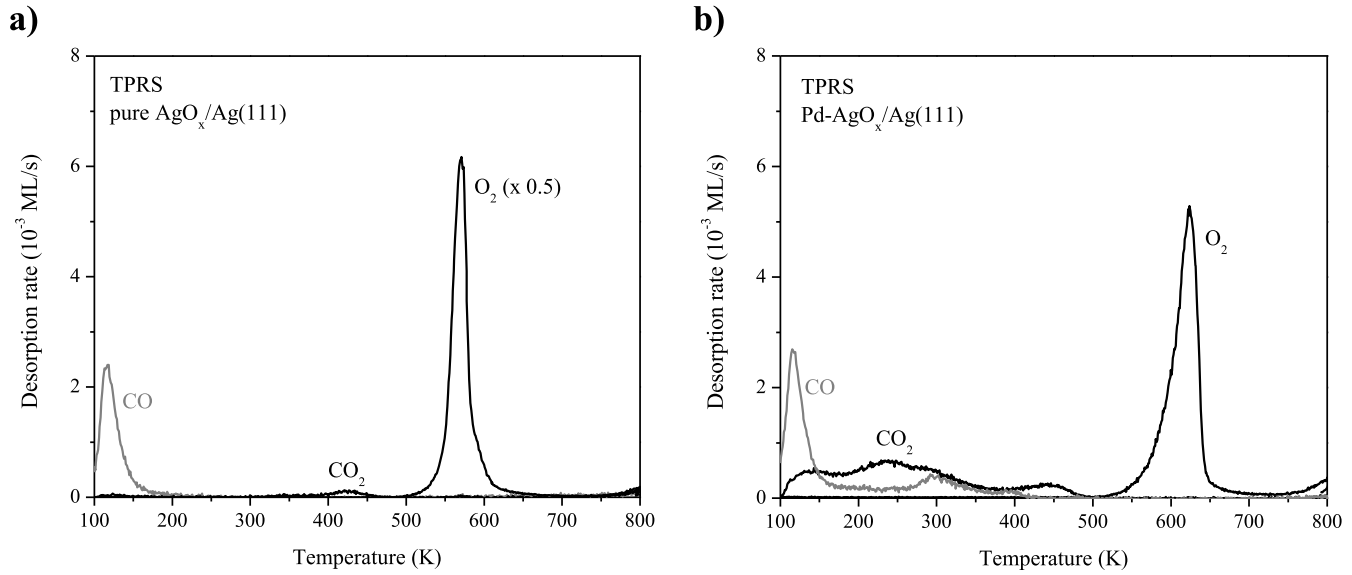

Figure 7. Temperature-programmed reaction of CO on (a) pure AgO_x/Ag(111) and (b) Pd-covered AgO_x/Ag(111) illustrates the change in kinetics and product distribution when Pd is present. The Pd-covered surface was prepared by depositing 0.30 ML of Pd at 300 K and each surface was exposed to CO at 100 K until reaching CO saturation.

the intensity of the CO−Pd−O band relative to the CO−Pd band would be low even when the majority of the adsorbed CO is bound as CO−Pd−O. The preference of O to bind to the edges of Pd particles at <1.8 ML is also demonstrated by the absence of CO absorption bands below 2000 cm^{-1}, indicating an absence of bridge-bound CO, as these sites are blocked by O. Clearly, O atoms shift toward terrace sites as the Pd clusters develop into a contiguous layer and eliminate edge sites. As a result, O and CO are forced to interact on the resulting surface, leading to an increasing fraction of the CO−Pd−O species on the terraces. This also corresponds to an appearance of bridge-bound CO (band near 1950 cm^{-1}), which are likely present to reduce coadsorbate repulsions at these relatively high adsorbate coverages. The variation of the CO−Pd−O and CO−Pd intensities with increasing Pd coverage provides compelling evidence that oxygen preferentially binds on the edges of Pd clusters during oxygen transfer from the AgO_x surface.

Surface Reactivity toward CO. A pristine AgO_x layer shows very little reactivity with CO adsorbed at 100 K. Heating the surface to 800 K reveals about 0.01 ML production of CO_2 near 425 K and the desorption of approximately 92% of the surface oxygen in a sharp O_2 peak at 570 K (Figure 7a). The O_2 TPD yield is only slightly less than that obtained from the pure AgO_x single layer without adsorbed CO (Supporting Information, Figure S1).[16,45,46] The desorption of CO at 115 K is indicative of weakly bound CO to Ag, apparently originating mainly from the edges of the sample (Supporting Information). These results are consistent with previous work showing that the $p(4 \times 4)$−AgO_x structure on Ag(111) is reduced by CO in an autocatalytic mechanism in which CO adsorbs on clean silver and reacts at the interfacial boundaries between the surface oxide and the clean Ag; that is, the oxide itself is unreactive.[5] Overall, the pure AgO_x single layer exhibits negligible CO oxidation activity for the conditions studied here.

In contrast, the AgO_x surface covered with 0.30 ML of Pd reacts readily with CO, evolving 0.14 ML of CO_2 in a broad band between 100 and 500 K after adsorption of CO at 100 K (Figure 7b). After scaling the CO_2 yield by the Pd surface coverage (0.18 ML-surfPd, Table 1), the amount of oxygen consumed by CO oxidation is estimated to be 0.74 ML/ML-surfPd. This value is nearly identical to the amount of oxygen that transferred to Pd after depositing a comparable amount of Pd onto AgO_x (Figure 3), demonstrating that CO oxidation is highly effective on these small Pd clusters and that only the oxygen that was initially associated with the Pd reacts with CO during TPRS. Unreacted CO is also evolved from the surface near 300 and 395 K, consistent with stronger binding of CO on Pd compared with AgO_x.[47] Based on the CO and CO_2 desorption yields, the initial CO coverage is about 3.5 times higher on the Pd-decorated versus pure AgO_x surface (0.28 vs 0.08 ML), indicating that the Pd enhances CO adsorption at 100 K. Only about 57% of the oxygen initially associated with the AgO_x layer desorbs as O_2 from the 0.3 ML Pd/AgO_x surface. The decrease in the amount of O_2 evolved (Figure 7 a,b) is commensurate with the increased amount of CO_2 formed. The O_2 and CO_2 yields with and without Pd demonstrate clearly that CO consumes a significant fraction of the oxygen originally associated with the AgO_x phase prior to Pd deposition.

The enhanced CO oxidation activity of Pd-covered versus pure AgO_x is attributed to the large fraction of Pd on the surface that oxidizes due to oxygen transfer from the AgO_x layer.[13] The O_2 TPD peak is also centered at a higher temperature (625 vs 570 K) on the 0.3 ML Pd-covered versus clean AgO_x surface, indicating that Pd stabilizes O atoms from the AgO_x phase. This finding is consistent with the stronger bonding of oxygen with Pd versus Ag that provides a thermodynamic driving force for the auto-oxidation of Pd by the AgO_x phase. A key finding is that CO oxidation occurs efficiently on Pd-covered AgO_x/Ag(111), even though the AgO_x phase is the only oxidant source.

The production of CO_2 at temperatures as low as 100 K further supports the conclusion that the oxygen transferred from AgO_x resides on the surfaces of the Pd clusters and that the combined coverage of adsorbed O and CO on the Pd is high (≥0.5 ML) after exposure to CO. Prior studies report that

https://dx.doi.org/10.1021/acscatal.0c03885
ACS Catal. XXXX, XXX, XXX−XXX

CO oxidation on oxygen-covered Pd surfaces occurs in three regions of temperature and coverage; reaction at combined CO and O coverages greater than 0.5 ML produces CO_2 between about 100 and 300 K, reaction at lower CO + O coverages produces CO_2 near 360 K, and reaction between isolated CO and O produces CO_2 near 420 K.[39,40,48] Analogous to the behavior reported for single-crystal Pd surfaces, the evolution of CO_2 from the Pd-covered AgO_x/Ag(111) surfaces also occurs approximately in three distinct temperature regimes (Figures 7b and S11a), with a significant amount of CO_2 produced below 300 K. The fact that CO_2 is produced on the Pd−AgO_x/Ag(111) surfaces at temperatures just above 100 K strongly suggests that O atoms are initially present on the Pd surfaces and thus available to react with adsorbed CO at low temperature.

Effect of Pd Coverage on CO Adsorption and Oxidation. The CO coverage resulting from saturation exposure to CO at 100 K increases with increasing Pd coverage on AgO_x until reaching a steady value of 0.72 ML on the surface fully covered by Pd (Figure 8a), in good agreement with the saturation coverage of CO on clean Pd(111) at 100 K.[47] The fact that the CO coverage at 2 ML Pd coverage is lower is attributed to site blocking by O atoms that migrated from the AgO_x layer to the surface of the Pd bilayer. The fact that the CO coverage increases in proportion to the fractional area of the surface covered by Pd (Table 1) is consistent with CO adsorbing at 100 K only on the Pd domains. The yield of CO_2 produced initially increases with Pd coverage and reaches a maximum as the Pd bilayer is nearly completed, the maximum CO_2 yield being approximately equal to the initial oxygen coverage (~0.38 ML) in the AgO_x layer. Concurrently, the yield of unreacted O_2 decreases to a negligible value (Figure 8a). These results show that nearly all of the oxygen atoms (>97%) from the AgO_x layer are consumed by CO oxidation when the Pd bilayer nearly completely covers the surface (2 ML Pd) and thus reveal that oxygen atoms from the buried Pd−AgO_x interface efficiently migrate through the Pd bilayer and react with CO adsorbed at the Pd surface. The CO IR spectra indicate that prior to CO adsorption, the oxygen migrates to the surface of the Pd bilayer during Pd deposition onto AgO_x at 300 K, which is consistent with the minimum energy structures predicted by DFT (Figures 4 and 5).

After Pd bilayer formation, however, the CO_2 yield decreases and becomes negligible at a Pd coverage near 4 ML, while the yield of desorbed O_2 continues to remain close to zero (Figure 8a). These observations indicate that O atoms originally associated with the AgO_x phase become increasingly unable to react with adsorbed CO or recombinatively desorb from the surface as the Pd layer thickens beyond 2 ML. Such behavior suggests that the oxygen remains trapped in the subsurface region as the temperature is increased to 800 K during TPRS. In support of this interpretation, surface IR spectra obtained after adsorbing CO at 100 K show that the surface oxygen coverage becomes negligible as the Pd coverage is increased to about 4.4 ML. As may be seen in Figure S10, bands from bridge-bound CO on metallic Pd intensify as the Pd coverage is increased above 2 ML and the CO−Pd−O band near 2140 cm^{-1} is absent in the spectrum obtained at a Pd coverage of ~4.4 ML, the spectrum closely resembling that obtained from pure Pd(111) after saturation with CO at 100 K. The lack of O_2 desorption is also consistent with prior studies, which show that temperatures above about 900 K are required to observe appreciable desorption of oxygen from the subsurface of Pd(111) during TPD.[49,50] A key finding is that oxygen migration to the surface of Pd domains is a highly facile process by which the AgO_x phase supplies O atoms to Pd, provided that the Pd domains are sufficiently thin (≤2 ML).

The oxygen consumed by CO oxidation clearly exceeds the amount of oxygen covered by the Pd bilayer domains for Pd coverages between 0.3 and 1.8 ML (Figure 8b) and exhibits a similar dependence on the Pd coverage as observed for the amount of oxygen transferred to the Pd prior to CO adsorption (Figure 3). An approximate comparison suggests that the oxygen consumed by CO oxidation is close to the

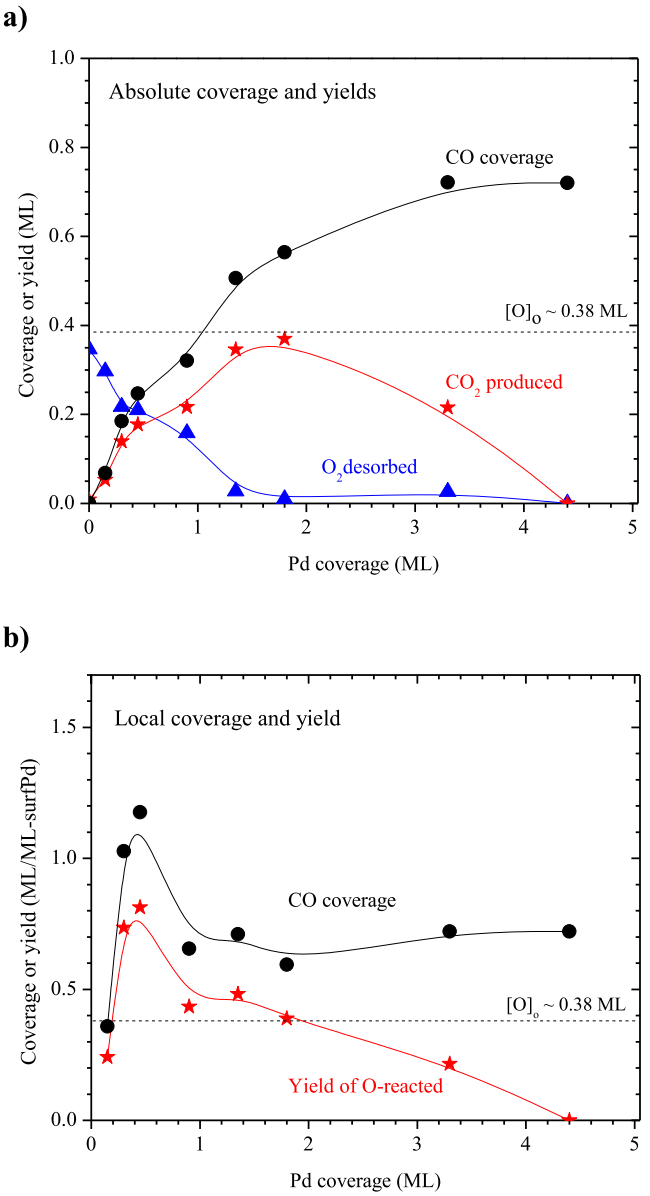

Figure 8. (a) Absolute initial CO coverage and the CO_2 and O_2 desorption yields (ML) and (b) local CO coverage and yield of O consumed by reaction (ML/ML-surfPd) as a function of the Pd coverage following CO saturation at 100 K. The initial CO coverage in (a) is given by the sum of the CO_2 and CO TPRS yields. CO, O_2, and CO_2 TPRS traces for all Pd coverages studied are shown in Figure S11, Supporting Information. Local coverages and yields are given in units of ML/ML-surfPd and determined by dividing the total yield or coverage by the surface Pd coverage (Table 1), after subtracting small contributions made from species desorption from uncovered AgO_x.

https://dx.doi.org/10.1021/acscatal.0c03885
ACS Catal. XXXX, XXX, XXX−XXX

initial oxygen coverage on the Pd; a comparison at each Pd coverage is not possible because of the differences in the Pd coverages examined with XPS versus CO TPRS. This result shows that CO oxidation is highly effective in removing oxygen from the Pd clusters but suggests that additional oxygen transfer from the AgO_x layer contributes negligibly to the oxidation of CO adsorbed at 100 K. An implication is that residual oxygen on the AgO_x surface is far removed from the Pd clusters and unable to diffuse rapidly enough to the Pd to react with CO on the timescale of the TPRS measurement. The larger quantities of CO_2 produced on small bilayer Pd clusters are clearly attributable to the higher initial coverages of oxygen on these clusters, which result from preferential binding of oxygen on edge sites of the Pd clusters and facile oxygen transfer from the AgO_x surface. Overall, the Pd−AgO_x/Ag(111) surfaces are highly active in CO oxidation because the AgO_x phase efficiently supplies oxygen to the Pd.

The ability of the small Pd bilayer clusters to accommodate large quantities of adsorbed CO also contributes to the enhanced production of CO_2 at low Pd coverages. The CO coverage and the amount of O consumed per ML of surface Pd track one another as the Pd coverage increases to 2 ML (Figure 8b), the CO coverage on small bilayer clusters increasing to greater than 1 ML/ML-surfPd when the amount of O consumed reaches a maximum. Prior studies show that supported metal nanoparticles can accommodate large CO coverages because the finite terrace widths allow the CO molecules to tilt away from one another, which greatly reduces oxygen−oxygen and dipole−dipole repulsions.[36,51,52] Preferential binding on edge sites can also enhance the CO coverage on metal nanoparticles of decreasing size. Accounting for Pd edge atoms, CO coverages at 100 K are estimated to be between ∼0.7 and 0.8 CO/Pd_{surf} for the ∼3 nm clusters at Pd coverages of 0.3 and 0.45 ML and decrease to 0.5 to 0.6 CO/Pd_{surf} for the larger domains that form as the Pd bilayer approaches completion (Section S4; Table S2). These CO coverages are larger than the fraction of edge sites estimated for 3 and 6 nm Pd clusters (0.50 vs 0.30 Pd_{edge}/Pd_{surf}), suggesting that CO adsorbs on both edge sites and terrace sites of the Pd clusters, in agreement with the results from surface IR spectroscopy (Figure 6). The ability of the small bilayer clusters to accommodate high coverages of CO is attributed to enhanced binding on Pd edge sites and, together with the higher oxygen coverages on the Pd, enables these clusters to produce CO_2 more effectively than large Pd domains.

Summary. The results of this study establish that coexisting Pd and AgO_x phases act cooperatively via a mechanism in which the AgO_x layer supplies O atoms to Pd domains and the O atoms oxidize CO adsorbed on the Pd. Oxygen migration from AgO_x to the Pd surface occurs facilely by two processes, namely, oxygen transfer to Pd at the buried Pd−AgO_x interface and diffusion of O atoms across the AgO_x surface to the Pd domains. Smaller bilayer clusters of Pd affect a higher efficiency of oxygen transfer from the AgO_x surface, as they can optimally incorporate interfacial oxygen as well as oxygen from the surrounding AgO_x. Enhanced stabilization of the oxygen causes the edges of Pd clusters to become enriched in oxygen and further promotes oxygen transfer to clusters of decreasing size. The oxygen coverage per Pd atom increases significantly as the Pd cluster size is decreased, reaching values that exceed the oxygen concentration in the AgO_x layer by as much as a factor 2. The preference for the transferred oxygen to bind on the edges of the Pd clusters was confirmed using several complementary methods, including quantitative analysis of XPS spectra, surface IR spectroscopy of adsorbed CO and DFT calculations of a Pd cluster supported on a AgO_x single layer, as well as quantitative estimates of the Pd morphology obtained from previously reported STM measurements.[13]

Quantification of the reactivity of adsorbed CO with the oxidized surface confirms that these oxygen transfer mechanisms are operative and demonstrates that the partially oxidized Pd bilayer domains are highly reactive toward CO. Nearly all of the oxygen atoms on AgO_x that associate with Pd during its deposition at 300 K are consumed by reaction with CO subsequently adsorbed onto the Pd at 100 K. The results of this study demonstrate that the higher oxophilicity of Pd versus Ag induces efficient oxygen transfer from AgO_x to Pd that renders the Pd highly active toward the oxidation of CO. Enhanced oxygen transfer to small Pd clusters and their subsequent higher CO oxidation activity further reveal that undercoordinated edge sites of the Pd clusters have higher oxygen concentrations and thus result in higher CO oxidation rates near the Pd and AgO_x interface. These findings clarify oxygen-exchange processes that may be broadly applicable in applications of oxidation chemistry promoted by bimetallic catalysts.

■ ASSOCIATED CONTENT

Supporting Information

The Supporting Information is available free of charge at https://pubs.acs.org/doi/10.1021/acscatal.0c03885.

Sample mounting and cleaning; O_2 TPD spectrum from single-layer AgO_x/Ag(111); structural models of single-layer AgO_x/Ag(111) phases; relationships between edge and terrace sites of bilayer Pd clusters; analysis of O 1s and Pd 3d spectra acquired from Pd deposited on AgO_x/Ag(111); DFT-computed energies of oxygen transfer to a Pd single layer; DFT-computed energies of O configurations on the Pd bilayer; additional O configurations on the Pd_{46} cluster on AgO_x; C−O stretch frequencies of CO on the Pd bilayer on AgO_x: influence of adsorbed O; CO RAIRS as a function of Pd coverage on AgO_x; and TPRS traces as a function of Pd coverage on AgO_x (PDF)

■ AUTHOR INFORMATION

Corresponding Author

Jason F. Weaver − *Department of Chemical Engineering, University of Florida, Gainesville, Florida 32611, United States;* orcid.org/0000-0002-6777-4727; Phone: 352-392-0869; Email: weaver@che.ufl.edu; Fax: 352-392-9513

Authors

Vikram Mehar − *Department of Chemical Engineering, University of Florida, Gainesville, Florida 32611, United States*

Abdulrahman Almithn − *Department of Chemical Engineering, University of Florida, Gainesville, Florida 32611, United States; Department of Chemical Engineering, King Faisal University, Al-Ahsa 31982, Saudi Arabia*

Tobias Egle − *Department of Chemistry and Chemical Biology and School of Engineering and Applied Sciences, Harvard University, Cambridge, Massachusetts 02138, United States;* orcid.org/0000-0003-1670-9754

https://dx.doi.org/10.1021/acscatal.0c03885
ACS Catal. XXXX, XXX, XXX−XXX

Ming-Hung Yu − *Department of Chemical Engineering, University of Florida, Gainesville, Florida 32611, United States*
Christopher R. O'Connor − *Department of Chemistry and Chemical Biology, Harvard University, Cambridge, Massachusetts 02138, United States*
Mustafa Karatok − *Department of Chemistry and Chemical Biology, Harvard University, Cambridge, Massachusetts 02138, United States*
Robert J. Madix − *School of Engineering and Applied Sciences, Harvard University, Cambridge, Massachusetts 02138, United States;* orcid.org/0000-0002-3132-2382
David Hibbitts − *Department of Chemical Engineering, University of Florida, Gainesville, Florida 32611, United States;* orcid.org/0000-0001-8606-7000
Complete contact information is available at: https://pubs.acs.org/10.1021/acscatal.0c03885

Author Contributions

[⊥]V.M. and A.A. contributed equally to this work.

Notes

The authors declare no competing financial interest.

■ ACKNOWLEDGMENTS

The authors thank Cynthia Friend for helpful technical discussions and Jeffrey Miller for editorial assistance. This work was supported as part of the Integrated Mesoscale Architectures for Sustainable Catalysis, an Energy Frontier Research Center funded by the U.S. Department of Energy, Office of Science, Basic Energy Sciences, under award no. DE-SC0012573. A.A. acknowledges Saudi Arabian Cultural Mission (SACM) and King Faisal University, Saudi Arabia, for funding his graduate studies and research. Computational resources were provided by the University of Florida Research Computing and the Extreme Science and Engineering Discovery Environment (XSEDE; CTS160041).

■ REFERENCES

(1) Weaver, J. F. Surface chemistry of late transition metal oxides. *Chem. Rev.* **2013**, *113*, 4164−4215.
(2) Wachs, I. E.; Madix, R. J. Oxidation of methanol on a silver (110) catalyst. *Surf. Sci.* **1978**, *76*, 531−558.
(3) Jones, G. S.; Barteau, M. A.; Vohs, J. M. Mechanism of diethyl ether formation on Ag(110) and its dependence on coadsorbed oxygen species. *J. Phys. Chem. B* **1999**, *103*, 1144−1151.
(4) Jones, G. S.; Barteau, M. A.; Vohs, J. M. The formation of diethyl ether via the reaction of iodoethane with atomic oxygen on the Ag(110) surface. *Surf. Sci.* **1999**, *420*, 65−80.
(5) Klust, A.; Madix, R. J. Mesoscopic restructuring and mass transport of metal atoms during reduction of the Ag(111)-p(4x4)-O surface with CO. *J. Chem. Phys.* **2007**, *126*, 084707.
(6) Hibbitts, D.; Neurock, M. Promotional effects of chemisorbed oxygen and hydroxide in the activation of C-H and O-H bonds over transition metal surfaces. *Surf. Sci.* **2016**, *650*, 210−220.
(7) Zhang, F.; Li, T.; Pan, L.; Asthagiri, A.; Weaver, J. F. CO oxidation on single and multilayer Pd oxides on Pd(111): mechanistic insights from RAIRS. *Catal. Sci. Tech.* **2014**, *4*, 3826−3834.
(8) Zhang, F.; Pan, L.; Li, T.; Diulus, J. T.; Asthagiri, A.; Weaver, J. F. CO oxidation on PdO(101) during temperature programmed reaction spectroscopy: Role of oxygen vacancies. *J. Phys. Chem. C* **2014**, *118*, 28647−28661.
(9) Weaver, J. F.; Zhang, F.; Pan, L.; Li, T.; Asthagiri, A. Vacancy-mediated processes in the oxidation of CO on PdO(101). *Acc. Chem. Res.* **2015**, *48*, 1515−1523.
(10) Weaver, J. F.; Choi, J.; Mehar, V.; Wu, C. Kinetic Coupling among Metal and Oxide Phases during CO Oxidation on Partially Reduced PdO(101): Influence of Gas-Phase Composition. *ACS Catal.* **2017**, *7*, 7319−7331.
(11) O'Connor, C. R.; Van Spronsen, M. A.; Egle, T.; Xu, F.; Kersell, H.; Oliver-Meseguer, J.; Karatok, M.; Salmeron, M.; Madix, R. J.; Friend, C. M. Hydrogen migration at restructuring palladium−silver oxide boundaries dramatically enhances reduction rate of silver oxide. *Nat. Commun.* **2020**, *11*, 1844.
(12) Karatok, M.; Egle, T.; Mehar, V.; O'Connor, C. R.; Yu, M.-H.; Friend, C. M.; Weaver, J. F. Reduction of Oxidized Pd/Ag(111) Surfaces by H_2: Sensitivity to PdO Island Size and Dispersion. *ACS Catal.* **2020**, *10*, 10117−10124.
(13) Mehar, V.; O'Connor, C. R.; Egle, T.; Karatok, M.; Madix, R. J.; Friend, C. M.; Weaver, J. F. Growth and auto-oxidation of Pd on single-layer AgO_x/Ag(111). *Phys. Chem. Chem. Phys.* **2020**, *22*, 6202−6209.
(14) Devarajan, S. P.; Hinojosa, J. A.; Weaver, J. F. STM study of high-coverage structures of atomic oxygen on Pt(111): p(2 x 1) and Pt oxide chain structures. *Surf. Sci.* **2008**, *602*, 3116−3124.
(15) Powell, C. J.; Jablonski, A. *NIST Electron Inelastic-Mean-Free-Path Database*. National Institute of Standards and Technology: Gaithersburg, Maryland 20899, 2010.
(16) Derouin, J.; Farber, R. G.; Turano, M. E.; Iski, E. V.; Killelea, D. R. Thermally Selective Formation of Subsurface Oxygen in Ag(111) and Consequent Surface Structure. *ACS Catal.* **2016**, *6*, 4640−4646.
(17) Schnadt, J.; Knudsen, J.; Hu, X. L.; Michaelides, A.; Vang, R. T.; Reuter, K.; Li, Z. S.; Laegsgaard, E.; Scheffler, M.; Besenbacher, F. Experimental and theoretical study of oxygen adsorption structures on Ag(111). *Phys. Rev. B: Condens. Matter Mater. Phys.* **2009**, *80*, 075424.
(18) Schnadt, J.; Michaelides, A.; Knudsen, J.; Vang, R. T.; Reuter, K.; Laegsgaard, E.; Scheffler, M.; Besenbacher, F. Revisiting the structure of the p(4x4) surface oxide on Ag(111). *Phys. Rev. Lett.* **2006**, *96*, 146101.
(19) Mehar, V.; Kim, M.; Shipilin, M.; Van den Bossche, M.; Gustafson, J.; Merte, L. R.; Hejral, U.; Grönbeck, H.; Lundgren, E.; Asthagiri, A.; Weaver, J. F. Understanding the intrinsic surface reactivity of single-layer and multilayer PdO(101) on Pd(100). *ACS Catal.* **2018**, *8*, 8553−8567.
(20) Kresse, G.; Hafner, J. Abinitio Hellmann-Feynman molecular-dynamics for liquid-metals. *J. Non-Cryst. Solids* **1993**, *156−158*, 956−960.
(21) Kresse, G.; Hafner, J. Ab-initio molecular-dynamics simulation of the liquid-metal amorphous-semiconductor transition in germanium. *Phys. Rev. B: Condens. Matter Mater. Phys.* **1994**, *49*, 14251−14269.
(22) Kresse, G.; Furthmüller, J. Efficient iterative schemes for ab initio total-energy calculations using a plane-wave basis set. *Phys. Rev. B: Condens. Matter Mater. Phys.* **1996**, *54*, 11169−11186.
(23) Kresse, G.; Furthmüller, J. Efficiency of ab-initio total energy calculations for metals and semiconductors using a plane-wave basis set. *Comput. Mater. Sci.* **1996**, *6*, 15−50.
(24) Kravchenko, P.; Plaisance, C.; Hibbitts, D. *A New Computational Interface for Catalysis*. 2019.
(25) Kresse, G.; Joubert, D. From ultrasoft pseudopotentials to the projector augmented-wave method. *Phys. Rev. B: Condens. Matter Mater. Phys.* **1999**, *59*, 1758−1775.
(26) Blöchl, P. E. Projector augmented-wave method. *Phys. Rev. B: Condens. Matter Mater. Phys.* **1994**, *50*, 17953−17979.
(27) Hammer, B.; Hansen, L. B.; Nørskov, J. K. Improved adsorption energetics within density-functional theory using revised Perdew-Burke-Ernzerhof functionals. *Phys. Rev. B: Condens. Matter Mater. Phys.* **1999**, *59*, 7413−7421.
(28) Perdew, J. P.; Burke, K.; Ernzerhof, M. Generalized gradient approximation made simple. *Phys. Rev. Lett.* **1996**, *77*, 3865−3868.
(29) Zhang, Y.; Yang, W. Comment on "Generalized gradient approximation made simple". *Phys. Rev. Lett.* **1998**, *80*, 890.
(30) Schmid, M.; Reicho, A.; Stierle, A.; Costina, I.; Klikovits, J.; Kostelnik, P.; Dubay, O.; Kresse, G.; Gustafson, J.; Lundgren, E.;

Andersen, J. N.; Dosch, H.; Varga, P. Structure of Ag(111)-p(4x4)-O: No silver oxide. *Phys. Rev. Lett.* **2006**, *96*, 146102.
(31) Martin, N. M.; Klacar, S.; Grönbeck, H.; Knudsen, J.; Schnadt, J.; Blomberg, S.; Gustafson, J.; Lundgren, E. High-Coverage Oxygen-Induced Surface Structures on Ag(111). *J. Phys. Chem. C* **2014**, *118*, 15324−15331.
(32) Wang, L.; Zeng, Z.; Gao, W.; Maxson, T.; Raciti, D.; Giroux, M.; Pan, X.; Wang, C.; Greeley, J. Tunable intrinsic strain in two-dimensional transition metal electrocatalysts. *Science* **2019**, *363*, 870−874.
(33) Monkhorst, H. J.; Pack, J. D. Special Points for Brillouin-Zone Integrations. *Phys. Rev. B: Solid State* **1976**, *13*, 5188−5192.
(34) Pack, J. D.; Monkhorst, H. J. "Special points for Brillouin-zone integrations"-a reply. *Phys. Rev. B: Solid State* **1977**, *16*, 1748−1749.
(35) Almithn, A. S.; Hibbitts, D. D. Supra-Monolayer Coverages on Small Metal Clusters and Their Effects on H-2 Chemisorption Particle Size Estimates. *AIChE J.* **2018**, *64*, 3109−3120.
(36) Liu, J.; Hibbitts, D.; Iglesia, E. Dense CO Adlayers as Enablers of CO Hydrogenation Turnovers on Ru Surfaces. *J. Am. Chem. Soc.* **2017**, *139*, 11789−11802.
(37) Wolter, K.; Seiferth, O.; Libuda, J.; Kuhlenbeck, H.; Bäumer, M.; Freund, H.-J. Infrared study of CO adsorption on alumina supported palladium particles. *Surf. Sci.* **1998**, *402*−*404*, 428−432.
(38) Frank, M.; Kühnemuth, R.; Bäumer, M.; Freund, H.-J. Vibrational spectroscopy of CO adsorbed on supported ultra-small transition metal particles and single metal atoms. *Surf. Sci.* **2000**, *454*−*456*, 968−973.
(39) Stuve, E. M.; Madix, R. J.; Brundle, C. R. Co Oxidation on Pd(100) - a Study of the Coadsorption of Oxygen and Carbon-Monoxide. *Surf. Sci.* **1984**, *146*, 155−178.
(40) Fukui, K.-i.; Miyauchi, H.; Iwasawa, Y. CO adsorption and oxidation on Pd(110)-c(2x4)-O by reflection-absorption infrared spectroscopy. *J. Phys. Chem.* **1996**, *100*, 18795−18801.
(41) Ma, Y.; Diemant, T.; Bansmann, J.; Behm, R. J. The interaction of CO with PdAg/Pd(111) surface alloys-A case study of ensemble effects on a bimetallic surface. *Phys. Chem. Chem. Phys.* **2011**, *13*, 10741−10754.
(42) Ma, Y.; Bansmann, J.; Diemant, T.; Behm, R. J. Formation, stability and CO adsorption properties of PdAg/Pd(111) surface alloys. *Surf. Sci.* **2009**, *603*, 1046−1054.
(43) Khan, N. A.; Uhl, A.; Shaikhutdinov, S.; Freund, H.-J. Alumina supported model Pd-Ag catalysts: A combined STM, XPS, TPD and IRAS study. *Surf. Sci.* **2006**, *600*, 1849−1853.
(44) Hoffmann, F. Infrared reflection-absorption spectroscopy of adsorbed molecules. *Surf. Sci. Rep.* **1983**, *3*, 107−192.
(45) Derouin, J.; Farber, R. G.; Heslop, S. L.; Killelea, D. R. Formation of surface oxides and Ag2O thin films with atomic oxygen on Ag(111). *Surf. Sci.* **2015**, *641*, L1−L4.
(46) Campbell, C. T. Atomic and Molecular-Oxygen Adsorption on Ag(111). *Surf. Sci.* **1985**, *157*, 43−60.
(47) Guo, X.; Yates, J. T. Dependence of Effective Desorption Kinetic-Parameters on Surface Coverage and Adsorption Temperature - Co on Pd(111). *J. Chem. Phys.* **1989**, *90*, 6761−6766.
(48) Conrad, H.; Ertl, G.; Küppers, J. Interactions between Oxygen and Carbon-Monoxide on a Pd(111) Surface. *Surf. Sci.* **1978**, *76*, 323−342.
(49) Kan, H. H.; Weaver, J. F. Mechanism of PdO thin film formation during the oxidation of Pd(111). *Surf. Sci.* **2009**, *603*, 2671−2682.
(50) Leisenberger, F. P.; Koller, G.; Sock, M.; Surnev, S.; Ramsey, M. G.; Netzer, F. P.; Klötzer, B.; Hayek, K. Surface and subsurface oxygen on Pd(111). *Surf. Sci.* **2000**, *445*, 380−393.
(51) Allian, A. D.; Takanabe, K.; Fujdala, K. L.; Hao, X.; Truex, T. J.; Cai, J.; Buda, C.; Neurock, M.; Iglesia, E. Chemisorption of CO and Mechanism of CO Oxidation on Supported Platinum Nanoclusters. *J. Am. Chem. Soc.* **2011**, *133*, 4498−4517.
(52) Loveless, B. T.; Buda, C.; Neurock, M.; Iglesia, E. CO Chemisorption and Dissociation at High Coverages during CO Hydrogenation on Ru Catalysts. *J. Am. Chem. Soc.* **2013**, *135*, 6107−6121.

https://dx.doi.org/10.1021/acscatal.0c03885
ACS Catal. XXXX, XXX, XXX−XXX